J Inorg Organomet Polym (2017) 27:1022–1027
DOI 10.1007/s10904-017-0550-8

# Anatase-Titania Templated by Nanofibrillated Cellulose and Photocatalytic Degradation for Methyl Orange

**He Xiao[1,2] · Junrong Li[1] · Beihai He[1]**

Received: 31 January 2017 / Accepted: 18 April 2017 / Published online: 27 April 2017


**Abstract** In this work, novel titania ($TiO_2$) nanoparticles were designed as a high performance photocatalyst. It was obtained by a simple method of dispersing nanofibrillated cellulose (NFC) onto the surface of titanium tetrachloride ($TiCl_4$), inducing crystallization and removing NFC templates. Under UV light irradiation, The $TiO_2$ nanoparticles displayed excellent photocatalytic activity for the decomposition of methyl orange solution. It was found that $TiO_2$ after calcination had a more efficiency than that before calcination. The optimum calcination temperature for the removal of NFC templates was 300 °C. Methyl orange solution had been remarkably degraded by $TiO_2$ nanoparticles when the mass ratio of $TiCl_4$ and NFC was 12:1. These results indicate that the $TiO_2$ nanopartilces can be easily applied in the field of wastewater treatment.

**Keywords** Nanofibrillated cellulose · Template · $TiO_2$ · Photocatalyst

## 1 Introduction

Morphology controllable inorganic metal oxide has successfully obtained by natural materials as template, demonstrating excellent properties and development of composites for application in photocalysis, energy, medicines and so on [1–5]. A series of natural templates containing cellulose, lignin, chitosan and alginate are used to fabricate functional materials [6–9]. Recently, cellulose has been widely applied to template-directed synthesize functional nanomaterials of metal oxide [10, 11].

Nanofibrillated cellulose is made of D-glucose monomers linked by β-1,4 ether linkages containing abundant hydroxyl and carboxyl groups and ether bonds which support affinities and active sites to the dispersion and growth of inorganic nanoparticles [12, 13]. Moreover, the extensive hydrogen bond network of nanofibrillated cellulose builds up an ordered structure for providing enough space with formation of metallic oxide [14, 15]. These hydroxyl groups on the surface of cellulose acting as efficient hydrophilic active sites can accelerate the growth of metallic oxide particles [16]. Nanofibrillated cellulose template content had effects on the surface morphology of nanoparticles. To obtain the pure titanium dioxide with highly active crystal phase, proper calcination temperature could be required.

In this paper, $TiO_2$ nanoparticles were successfully synthesized by using nanofibrillated cellulose as a template. The chemical composition, crystallinity and morphology of $TiO_2$ were investigated by Fourier Transform Infrared Spectroscopy (FT-IR), Thermo Gravimetric Analyzer (TGA) and Scanning Electron Microscope (SEM), respectively. Effects of calcination temperature and template content on photocatalytic degrading methyl orange were investigated.

✉ He Xiao
xiaohe_river@163.com

[1] College of Materials Engineering, Fujian Agriculture and Forestry University, Fuzhou 350002, China

[2] State Key Laboratory of Pulp and Paper Engineering, South China University of Technology, Guangzhou 510641, China

## 2 Experimental

### 2.1 Materials

Titanium tetrachloride, hydrochloric acid, ammonium sulphate, ammonia and absolute alcohol were of analytical grade and utilized without purification. Nanofibrillated cellulose (NFC) was obtained from Guilin Qihong Science and Technology Co., Ltd (0.6 wt%, average length: 6.8 nm, average width: 1000 nm).

### 2.2 Preparation of $TiO_2$ Nanoparticles with Nanofibrillated Cellulose

Four milliliter $TiCl_4$ (36 mmol) was added into 200 ml deionized water containing 1 g nanofibrillated cellulose (6.17 mmol) under continuous stirring in ice bath. After 1 h, 0.5 g $(NH_4)_2SO_4$ (3.79 mmol) and 1.58 ml HCl (18.96 mmol) were added dropwise with further stirring for 1 h in ice bath. Moreover, the mixture was warmed in an oil bath at 70 °C for 2 h. Then, the pH of the mixture was regulated to nearly eight using ammonia and stirring at room temperature for further 24 h. The obtained products were washed with deionized water and absolute ethanol, respectively. The purified products were calcined at 300, 400, 500 and 600 °C in air atmosphere for 4 h, respectively.

### 2.3 Characterizations

The Fourier transform infrared spectra were carried out on a spectrophotometer (Bruker, VERTEX70, Germany). The chemical compositions of $TiO_2$ and nanofibrillated cellulose template were measured by energy dispersive spectroscopy (HORIBA, XMX 1011, Japan). The morphologies of the products were observed using scanning electron microscope (Hitachi, SU8010, Japan). The thermal stabilities were evaluated using thermal gravimetric analysis (TA, Q500, USA). Samples were heated in an aluminum crucible to 700 °C at a heating rate of 10 °C/min. The crystal structure of $TiO_2$ was characterized by using X-ray diffraction analysis (Rigaku, Ultima IV, Japan) with Cu Kα radiation. Antase to rutile ratio was estimated from integrated intensities of the reflection of (101) and (110) phases [17]. The crystallite size of anatase and rutile was calculated according to the Scherrer formula. BET surface area of $TiO_2$ was characterized by nitrogen adsorption (Micromeritics, ASAP 2020, USA).

### 2.4 Evaluation of Photocatalytic Activity

The photocatalytic activity of $TiO_2$ nanoparticles was estimated using methyl orange solution as target degradation molecule. The photocatalytic source was launched out by ultraviolet lamp with power about 36 W. A mixture containing 25 mg of $TiO_2$ nanoparticles and 100 ml methyl orange (5 mg/l) was stirred for 30 min in the dark to reach adsorption equilibrium. Then, 3.5 ml of the mixture under UV irradiation was collected and filtered by 0.22 μm membrane at 15, 30, 60, 90 and 120 min, respectively. The absorbance of the filtrate was measured by UV–Vis spectrophotometer (Shimadzu, UVmini-1240, Japan).

## 3 Results and Discussion

### 3.1 Characteristics of $TiO_2$ Nanoparticles Templated by Nanofibrillated Cellulose

Obvious differences in wave numbers and intensities of the absorption bands can be observed between the spectra of $TiO_2$ templated by NFC as shown in Fig. 1. The peak at 3430 $cm^{-1}$ corresponds to stretching vibrations of hydroxyl groups of nanofibrillated cellulose. Loading $TiO_2$ nanoparticles on the nanofibrillated cellulose, peak of hydroxyl groups shift to 3216 $cm^{-1}$. After calcination, hydroxyl groups at 3373 $cm^{-1}$ are stronger than nano cellulose, which indicates that hydroxyl groups of nano cellulose have some interactions with both $Ti^{4+}$ and $TiO_2$ nanoparticles. A similar phenomenon was observed for the in-plane OH deformation vibration (1609–1605, 1624 and 1627 $cm^{-1}$, respectively).

The thermal properties of $TiO_2$ templated by NFC were conducted with TGA. Figure 2 shows the thermal gravimetric curves for $TiO_2$ with a heating rate of 10 °C/min under a nitrogen atmosphere. For NFC, the weight loss was 10.9% below 100 °C due to the moisture content in the NFC

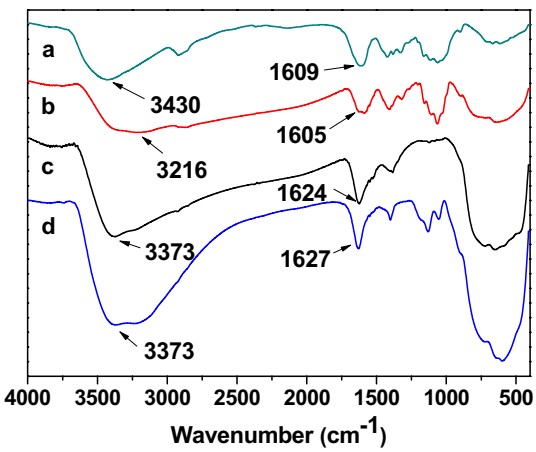


**Fig. 1** Fourier transformation infrared (FT-IR) spectra of $TiO_2$ templated by NFC [*a* NFC, *b* $TiO_2$ (3:1) (before calcination), *c* $TiO_2$ (3:1) (after 300 °C calcination), *d* $TiO_2$ without NFC template (after 300 °C calcination)]

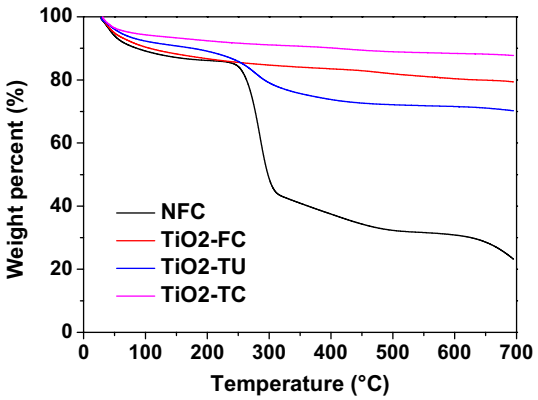


**Fig. 2** Thermogravimetric analysis for $TiO_2$ templated by NFC. ($TiO_2$-TU, [$TiO_2$ (3:1) before calcination); $TiO_2$-FC, after 300 °C calcination without NFC; $TiO_2$-TC, ($TiO_2$ (3:1) after 300 °C calcination]). (Color figure online)

sample. NFC began with rapid chemical decomposition at 238 °C, leaving 23.5% quality content at 700 °C. Regarding to $TiO_2$-FC, $TiO_2$-TU and $TiO_2$-TC, the weight loss below 100 °C were only 9.7, 7.7 and 5.7%, respectively. The quality content of $TiO_2$-TU (29.4%) was higher than $TiO_2$-FC (20.4%) and $TiO_2$-TC (12.1%) at 700 °C, which indicated that much of organic compounds coming from NFC remained in the $TiO_2$.

Figure 3 shows the SEM images of $TiO_2$ free of template and $TiO_2$ templated by NFC. From the SEM images, particle size of $TiO_2$ was about 200 nm regardless of template. $TiO_2$ free of template demonstrated that the $TiO_2$ nanoparticles were spherical shape. While $TiO_2$ templated by NFC showed that $TiO_2$ particles agglomerated into linear shape.

### 3.2 Effect of Calcination Temperature on the Photocatalytic Activity of $TiO_2$ Nanoparticles

The photocatalytic abilities of the obtained $TiO_2$ nanoparticles at different calcined temperatures were investigated by decomposing the methyl orange solution with the concentration of 5 mg/l. The obtained $TiO_2$ nanoparticles displayed superior photocatalytic activities, when the NFC template was removed. Residual concentration of methyl orange was reduced as the photocatalytic time. When the photocatalytic time was 60 min, the photodegradation efficiencies of the $TiO_2$ samples calcined at 300, 400, 500, 600 °C are about 95.7, 69.5, 64.7, 60.0%, respectively. As the photocatalytic time extended to 120 min, the methyl orange was removed above 96% (Fig. 4).

XRD diffraction patterns of $TiO_2$ nanoparticles calcined at different temperatures were shown in Fig. 5. The diffraction peaks at 2θ values of 25.3°, 27.4°, 37.0°, 37.8°, 41.4°, 48.1°, 53.9°, 55.1°, 62.7°, 68.8°, 70.4° and 75.0° correspond to the (101), (110), (101), (004), (111), (200), (105), (211), (204), (301), (112) and (215) planes of $TiO_2$, respectively, and readily be indexed to the anatase phase (JCPDS card No. 21-1272) and rutile phase (JCPDS card No. 65–0191). Calcinaed temperature had not affected the peak positions at 25.3° and 27.4° of anatase and rutile, respectively. But the anatase/rutile ratio had been slightly reduced with the calcined temperature as shown in Table 1. At the same time, the crystallite size of $TiO_2$ became larger

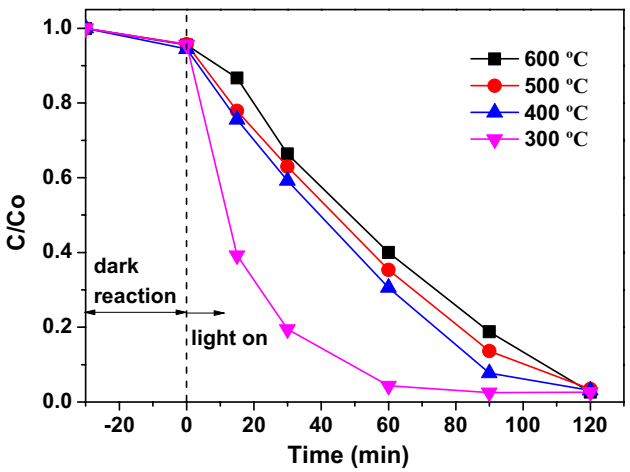


**Fig. 4** Photocatalytic activity of $TiO_2$ templated by NFC with different calcined temperatures

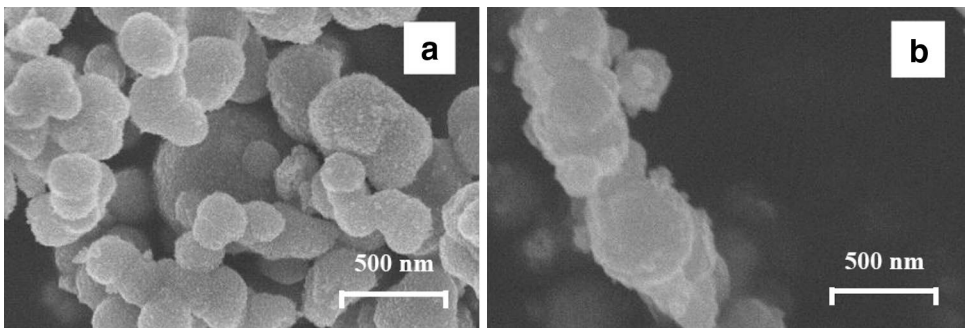


**Fig. 3** SEM images of **a** $TiO_2$ free of template (after 300 °C calcination) and **b** $TiO_2$ templated by NFC [$TiO_2$ (3:1), after 300 °C calcination]

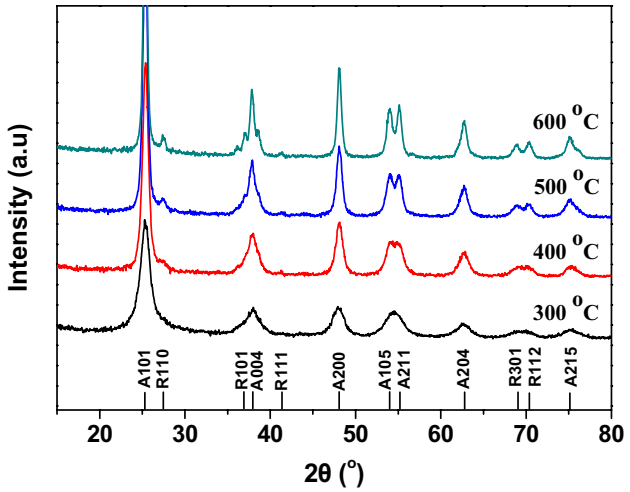


**Fig. 5** XRD patterns of $TiO_2$ calcined at different temperatures

**Table 1** Characteristics of the $TiO_2$ templated by NFC

| Calcined temperature (°C) | Anatase/rutile ratio | Crystallite size of anatase (A) rutile (R) (nm) | Surafce area ($m^2$/g) |
|---|---|---|---|
| 300 | 1 | A = 5.7 | 62.1 |
| 400 | 0.98 | A = 10.4; R = 16.2 | 50.3 |
| 500 | 0.96 | A = 13.6; R = 14.6 | 43.7 |
| 600 | 0.95 | A = 17.7; R = 21.8 | 29.8 |

$TiO_2$ (3:1)

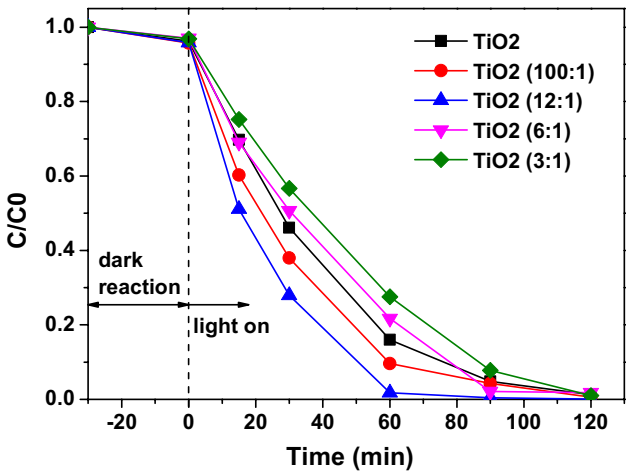


**Fig. 6** Photocatalytic activity of $TiO_2$ templated by NFC with different mixture ratios

with the calcined temperature. But the surface area of $TiO_2$ nanoparticles was getting smaller with the calcination temperature.

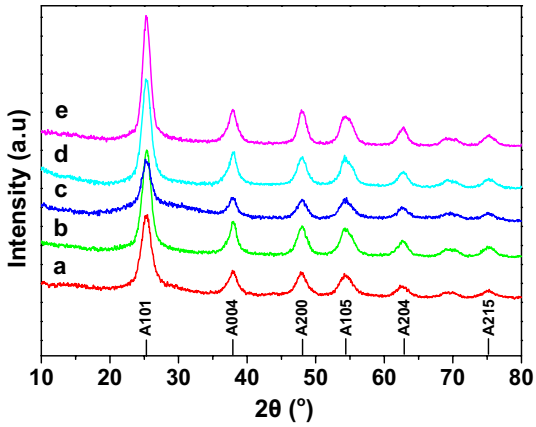


**Fig. 7** XRD patterns of $TiO_2$ templated with NFC *a* $TiO_2$, *b* $TiO_2$ (3:1), *c* $TiO_2$ (6:1), *d* $TiO_2$ (12:1), *e* $TiO_2$ (100:1)

### 3.3 Effect of Template Amount on the Photocatalytic Activity of $TiO_2$ Nanoparticles

Photocatalytic activities of $TiO_2$ templated by NFC with different mixture ratios were studied as shown in Fig. 6. After 120 min-UV irradiation, the decomposition ratio of methyl orange were all nearly 100% indicating that these $TiO_2$ had very strong photocatalytic activities. When the UV irradiation time was 60 min, the concentration of methyl orange was only 1.7% under the UV irradiation by $TiO_2$ (12:1). While other $TiO_2$ displayed the weak photocatalytic activities as the following order: $TiO_2$ (12:1) > $TiO_2$ (100:1) > $TiO_2$ > $TiO_2$ (6:1) > $TiO_2$ (3:1).

Figure 7 showed the X-ray diffraction data (XRD) of all the prepared materials which corresponded to $TiO_2$ (anatase) (JCPDS card NO. 21-1272). The diffraction peaks at 2θ values of 25.3°, 37.9°, 48.0°, 54.2°, 62.7° and 75.3° correspond to the (101), (004), (200), (105), (204), and (215) planes of $TiO_2$, respectively. From Table 2, the anatase/rutile ratio remained at 1, indicating that the $TiO_2$ was made from pure crystal phase of anatase. Crystallite size of all the $TiO_2$ nanoparticles was nearly 5 nm, while the surface area of $TiO_2$ nanoparticles varied with the different ratio between $TiCl_4$ and NFC. When the ratio between $TiCl_4$ and NFC was 12:1, the surface area of $TiO_2$ nanoparticles ran up to 88.3 $m^2$/g.

### 3.4 Reusability of $TiO_2$ Nanoparticles on Photocatalytic Activity

The reusability is an important parameter related to the application potential of photocatalysts. In this study, 25 mg of $TiO_2$ nanoparticles were added into 100 ml of methyl orange solution (5 mg/l) to measure the concentration of methyl orange after 30 and 60 min UV irradiation. As seen from Fig. 8, the resulted $TiO_2$ nanoparticles were used for

**Table 2** Characteristics of the $TiO_2$ templated by NFC

| Ratio | Anatase/ rutile ratio | Crystallite size of anatase (A) rutile (R) (nm) | Surafce area ($m^2/g$) |
|---|---|---|---|
| $TiO_2$ | 1 | A = 4.9 | 70.5 |
| $TiO_2$ (3:1) | 1 | A = 5.3 | 60.1 |
| $TiO_2$ (6:1) | 1 | A = 5.1 | 71.2 |
| $TiO_2$ (12:1) | 1 | A = 5.5 | 88.3 |
| $TiO_2$ (100:1) | 1 | A = 6.2 | 76.9 |

Calcination temperature was 300 °C

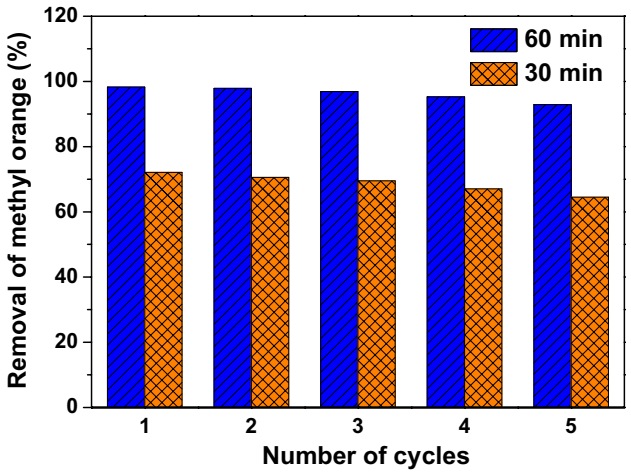


**Fig. 8** Reuasability of $TiO_2$ nanoparticles on photocatalytic activity [$TiO_2$ (12:1), calcinations temperature: 300 °C]

five cycles. The concentration of methyl orange had been still reduced above 90% (60 min UV irradiation) and 65% (30 min UV irradiation) after five batches. Thus, it is believed that it can be recycled for many times.

## 4 Conclusions

$TiO_2$ photocatalyst was synthesized by a hydrothermal approach with NFC as a template. The results showed that the catalytic activity of $TiO_2$ templated by NFC was more superior than $TiO_2$ free of template. When the calcination temperature was 300 °C, $TiO_2$ nanoparticles achieved the higher content of anatase phase with larger surface area in favor of photocatalytic degrading pollutant molecules. $TiO_2$ nanoparticles had the same content of anatase phase and crystallite size as the different ratios between $TiCl_4$ and NFC. $TiO_2$ templated by NFC exhibited a very good performance in removing methyl orange as well as a good reusability.

**Acknowledgements** This work was supported by State Key Laboratory of Pulp and Paper Engineering (201617), Fujian Science and Technology of Education Department Fund (JAT160151), Fujian Innovation and Entrepreneurship Training Program (201610389083).

## References

1. Y.Y. Kim, C. Neudeck, D. Walsh, Biopolymer templating as synthetic route to functional metal oxide nanoparticles and porous sponges. Polym. Chem. **1**(3), 272–275 (2010)
2. B. Boury, S. Plumejeau, Metal oxides and polysaccharides: an efficient hybrid association for materials chemistry. Green Chem. **17**(1), 72–88 (2015)
3. A. Ivanova, D. Fattakhova-Rohlfing, B.E. Kayaalp et al., Tailoring the morphology of mesoporous titania thin films through biotemplating with nanocrystalline cellulose. J. Am. Chem. Soc. **136**(16), 5930–5937 (2014)
4. J.H. Kim, J.H. Kim, E.S. Choi et al., Colloidal silica nanoparticle-assisted structural control of cellulose nanofiber paper separators for lithium-ion batteries. J. Power Sources **242**, 533–540 (2013)
5. F.Y. Fu, L.Y. Li, L.J. Liu et al., Construction of cellulose based ZnO nanocomposite films with antibacterial properties through one-step coagulation. ACS Appl. Mater. Interfaces **7**(4), 2597–2606 (2015)
6. M.A. Mohamed, W. Salleh, J. Jaafar et al., Incorporation of N-doped $TiO_2$ nanorods in regenerated cellulose thin films fabricated from recycled newspaper as a green portable photocatalyst. Carbohydr. Polym. **133**, 429–437 (2015)
7. X.Y. Chen, D.H. Kuo, D.F. Lu et al., Synthesis and photocatalytic activity of mesoporous $TiO_2$ nanoparticle using biological renewable resource of un-modified lignin as a template. Microporous Mesoporous Mater. **223**, 145–151 (2016)
8. J. Liu, W.Y. Li, Y.G. Liu et al., Titanium(IV) hydrate based on chitosan template for defluoridation from aqueous solution. Appl. Surf. Sci. **293**, 46–54 (2014)
9. M.C. Kimling, R.A. Caruso, Sol–gel synthesis of hierarchically porous $TiO_2$ beads using calcium alginate beads as sacrificial templates. J. Mater. Chem. **22**(9), 4073–4082 (2012)
10. A. Henry, S. Plumejeau, L. Heux et al., Conversion of nanocellulose aerogel into $TiO_2$ and $TiO_2$@C nano-thorns by direct anhydrous mineralization with $TiCl_4$. Evaluation of electrochemical properties in Li batteries. ACS Appl. Mater. Interfaces **7**(27), 14584–14592 (2015)
11. B. Boury, R.G. Nair, S.K. Samdarshi et al., Non-hydrolytic synthesis of hierarchical $TiO_2$ nanostructures using natural cellulosic materials as both oxygen donors and templates. New J. Chem. **36**(11), 2196–2200 (2012)
12. H. Ceylan, C. Ozgit-Akgun, T.S. Erkal et al., Size-controlled conformal nanofabrication of biotemplated three-dimensional $TiO_2$ and ZnO nanonetworks. Sci. Rep. **3**, 1–7 (2013)
13. D.H. Yu, X.D. Yu, C.H. Wang et al., Synthesis of natural cellulose-templated $TiO_2$/Ag nanosponge composites and photocatalytic properties. ACS Appl. Mater. Interfaces **4**(5), 2781–2787 (2012)
14. Z.D. Li, C.H. Yao, F. Wang et al., Cellulose nanofiber-templated three-dimension $TiO_2$ hierarchical nanowire network for photoelectrochemical photoanode. Nanotechnology **25**(50), 1–10 (2014)
15. Y. Lu, Q.F. Sun, T.C. Liu et al., Fabrication, characterization and photocatalytic properties of millimeter-long $TiO_2$ fiber with nanostructures using cellulose fiber as a template. J. Alloys Compd. **577**, 569–574 (2013)

16. N. Olaru, G. Galin, L. Olaru, Zinc oxide nanocrystals grown on cellulose acetate butyrate nanofiber mats and their potential photocatalytic activity for dye degradation. Indus. Eng. Chem. Res. **53**(46), 17968–17975 (2014)

17. B. Tryba, A.W. Morawski, M. Inagaki, A new route for preparation of $TiO_2$-mounted activated carbon. Appl. Catal. B **46**(1), 203–208 (2003)